Carbohydrate Polymer Technologies and Applications 9 (2025) 100724

Contents lists available at ScienceDirect

Carbohydrate Polymer Technologies and Applications

journal homepage: www.sciencedirect.com/journal/carbohydrate-polymer-technologies-and-applications

Harnessing handheld inkjet printing technology for rapid and decentralised fabrication of drug-loaded hydroxypropyl cellulose buccal films

Paola Carou-Senra [a], Atheer Awad [b], Abdul W. Basit [c,d], Carmen Alvarez-Lorenzo [a,*], Alvaro Goyanes [a,c,d,*]

[a] Departamento de Farmacología, Farmacia y Tecnología Farmacéutica, I+D Farma (GI-1645), Facultad de Farmacia, Instituto de Materiales (iMATUS) and Health Research Institute of Santiago de Compostela (IDIS), Universidade de Santiago de Compostela, 15782 Santiago de Compostela, Spain
[b] Department of Clinical, Pharmaceutical and Biological Sciences, University of Hertfordshire, College Lane, Hatfield AL10 9AB, UK
[c] Department of Pharmaceutics, UCL School of Pharmacy, University College London, 29-39 Brunswick Square, London WC1N 1AX, UK
[d] FABRX Ltd., Henwood House, Henwood, Ashford, Kent TN24 8DH, UK

ARTICLE INFO

Keywords:
Buccal films
Drug printing on-demand
Handheld inkjet printing
Personalized medicine
Hydroxypropyl cellulose

ABSTRACT

Inkjet printing is emerging as a valuable tool for personalised medicine, offering precision and flexibility in pharmaceutical development. Efforts have been made to modify commercial desktop printers; however, the growing interest in decentralized and on-demand pharmaceutical production highlights the need for more compact, energy-efficient alternatives that enhance versatility and seamless integration across diverse environments. This study presents for the first time, a handheld inkjet printer for the portable production of personalised medications in decentralised settings using hydroxypropyl cellulose (HPC) films as the printing substrate. The compact design of handheld printers ensures ease of use, space efficiency, and reduced energy consumption, making them ideal for patient-centric applications. As a proof of concept, the Selpic S1+ handheld inkjet printer was used to create buccal films with flexible nicotine doses tailored for nicotine replacement therapy. By modifying the printed area and number of pharma-ink (drug-loaded pharmaceutical ink) layers, precise nicotine dosages were achieved. The films exhibited controlled drug release, strong mucoadhesive properties, and adequate mechanical properties for buccal application. Studies on swelling behaviour, mucoadhesion, and surface morphology validated the film structural integrity and functionality. *Ex vivo* permeation studies using porcine buccal mucosa demonstrated high nicotine permeability. Additionally, pharma-ink printing was successfully applied to other biological macromolecules substrates (starch and cellulose), underscoring the versatility of handheld devices in creating diverse patterns across different surfaces. This research highlights the potential of handheld inkjet printing on eco-friendly films for decentralised, rapid and affordable treatment customisation with improved therapeutic outcomes and patient adherence.

1. Introduction

The landscape of pharmaceutical manufacturing is undergoing a transformative shift with the integration of advanced technologies. These innovations are paving the way for a future where medications can be produced on demand, tailored specifically to the unique therapeutic needs of each patient. One of the most promising of these technologies is additive manufacturing (Tracy et al., 2023), which is poised to transform drug formulation by enabling the creation of personalised, small-batch medicines. This approach is particularly advantageous for drugs with narrow therapeutic windows or significant inter-individual variability (Krueger et al., 2024), ensuring that treatments are not only effective but also safer for patients.

Among the various printing methods, inkjet printing (IJP) stands out for its high precision and versatility. IJP operates by selectively depositing small liquid drops through a nozzle onto a substrate, offering unparalleled control and minimal material waste (Carou-Senra et al., 2024). IJP can be classified into two techniques based on how the ink drops are generated: continuous inkjet printing (CIJP) and drop-on-demand (DoD) IJP. The DoD techniques, which include thermal and piezoelectric printheads, respond to an electrical stimulus to eject small volumes of liquid and have emerged as a precise and flexible

* Corresponding authors.
E-mail addresses: carmen.alvarez.lorenzo@usc.es (C. Alvarez-Lorenzo), a.goyanes@fabrx.co.uk, a.goyanes@ucl.ac.uk (A. Goyanes).

https://doi.org/10.1016/j.carpta.2025.100724

Available online 20 February 2025

alternative for pharmaceutical development individualised medications with specific dosages (Sandler et al., 2011), combining multiple drugs into single forms (G. Eleftheriadis et al., 2020), designing controlled-release systems (Genina et al., 2012), and fabricating intricate drug delivery devices to optimise therapeutic outcomes (Fox et al., 2017). Notably, IJP has demonstrated significant potential in the development of oral films, which are conventionally manufactured using solvent casting technique (Kumria, Nair, Goomber & Gupta, 2016; Semalty, Semalty & Kumar, 2008). This traditional approach involves mixing the active pharmaceutical ingredient (API) and excipients in solution/suspension and casting the mixture into moulds. This approach often results in batch variability and limited control over the deposited dose (Carou-Senra et al., 2024). In contrast, IJP enables the independent deposition of the pharmaceutical-grade inks containing APIs, termed pharma-ink, onto a preproduced substrate, ensuring precise dose control through its drop-on-demand, non-contact mechanism (Carou-Senra et al., 2024). Research studies has focused on modifying and implementing commercial desktop inkjet printers by replacing the standard ink with pharma-inks and deposit it onto various substrates (Buanz, Saunders, Basit & Gaisford, 2011), using a wide range of drug, including biologics (G. Eleftheriadis et al., 2020; Montenegro-Nicolini, Miranda & Morales, 2017; G.K. Eleftheriadis et al., 2020; Alomari et al., 2018). Commercial desktop inkjet printing systems remain the primary focus, however the demand for decentralized and on-demand manufacturing highlights the need for more compact, energy-efficient solutions that enhance production flexibility using different substrates and resource optimization.

The advent of handheld inkjet printers has advanced the innovation of IJP further, offering unique advantages over traditional stationary desktop printers. Compact and lightweight, these portable devices are easy to carry and use anywhere, enabling mobile, on-the-go printing while conserving space and energy (Hang, 2014). Originally designed for printing barcodes and labels on various surfaces, handheld printers demonstrate remarkable versatility, capable of depositing ink onto nearly any substrate. Handheld devices often support wireless connections, such as Bluetooth or Wi-Fi, allowing users to print without being tethered to cables or reliant on continuous power supplies (Hang, 2014). This feature contrasts with larger desktop printers, which require constant power connections. Additionally, many handheld printers come equipped with dedicated software for creating designs, while wireless connectivity facilitates seamless integration of custom designs. These devices also offer impressive printing speeds, enhancing productivity in fast-paced environments where immediate solutions are required. Despite their small size, handheld inkjet printers maintain high print quality, ensuring precise ink deposition and excellent resolution of printed patterns. Handheld inkjet printers present a promising alternative to desktop models, unlocking new possibilities within the framework of 5Ps medicine (Predictive, Preventive, Participatory, Personalised, and Precision) (Gardes et al., 2019). Their portability and efficiency make them particularly suited for on-demand medicine production especially for films, even in remote or resource-limited settings, where decentralised and immediate solutions are essential. Despite this high potential, handheld inkjet printers have yet to be tested for the preparation of personalized medicines. Moreover, the full development of this 2D printing technology demands substrates that withstand the deposition of the required drug(s) dose(s) by applying one or more layers of pharma-ink. The development of versatile edible substrates using sustainable materials and applying green technologies is necessary for patient access and affordability of this decentralized (local) production of medicines by healthcare systems (Vogler et al., 2024). Indeed, World Health Organization (WHO) resolutions strongly insist on the need to develop strategies to ensure local production of essential medicines and other healthcare products to overcome shortages and improve equitable access regardless of country and geopolitical conditions (WHO 2025).

To highlight the value of handheld printing, we selected nicotine as a model drug due to its critical role in smoking cessation therapies. Nicotine replacement therapy works by reducing motivation to consume tobacco through delivery of small doses of nicotine. Various products are available on the market, primarily gums and lozenges, with fixed doses between 2 and 4 mg, commonly. However, these pharmaceutical forms present several disadvantages. Gums and lozenges are intended to be buccal forms, but may not be very effective, since a significant amount of the nicotine is swallowed, undergoing heavy first-pass hepatic metabolism (Suksaeree et al., 2021; Olsson Gisleskog et al., 2021). Patches, another common form of nicotine replacement therapy, often report local skin reactions (related with allergies), insomnia and also may not keep urgent cravings under control (A.C. Society 2021). Clinical strategies for nicotine replacement therapy still need improvement, in terms of effectivity, usage duration, dosing, and personalisation considering both external factors such as their level of nicotine dependence and individual smoker profiles (e.g., genotype, phenotype and sex) (Carpenter et al., 2013). Research indicates that optimal dosing varies with individual patient factors such as genotype, phenotype, and sex (Flowers, 2017), with women often requiring higher doses due to faster nicotine metabolism (Allen et al., 2019; Kosmider et al., 2018; Schnoll, Patterson & Lerman, 2007). This type of therapy must support the patient throughout their cessation journey, adjusting the dose according to each individual's needs while gradually decreasing it (NHS). The body needs to adapt to the nicotine diminishing levels, lowering the risk of relapses or suffering withdrawal syndrome. Such a personalised and gradual therapy cannot be effectively achieved with fixed and standard marketed doses.

In this proof-of-concept work, a handheld inkjet printer was employed for the rapid fabrication of buccal films with flexible and customisable drug doses (Fig. 1). Compared to previous literature on 2D printing and buccal films, two main innovations were introduced to preserve affordability and eco-friendly approach: (a) the ink was made as simple as possible by mixing the oily drug with water in the absence of any other excipients; and (b) the film was prepared by combining hydroxypropyl cellulose (HPC) with Eudragit NE 30D to regulate the mechanical properties and swelling of the film during printing and the subsequent control of drug release after administration; such combination allowed to skip the chemical cross-linking typical of cellulose ethers films, saving time and chemicals. Combination of cellulose ethers and polymethacrylates has been previously tested for other varieties and using organic solvents (Meher et al., 2013).

Notably, this study aims to (1) implement for the first time a handheld inkjet printer system to decentralise personalised drug product development, (2) characterise the performance of nicotine-loaded buccal films, and (3) investigate the application of this novel inkjet system onto other substrates. To carry out the work, a Selpic S1+ inkjet printer was tested for the flexible deposition of different doses of nicotine onto previously prepared films by varying the printed area and number of layers applied to the films. The study included comprehensive characterisations to ensure the reliability and applicability of the printed buccal films. Drug content analysis was conducted to assess the accuracy and reproducibility of drug deposition using this portable device. Mechanical properties were evaluated for structural integrity and buccal application post-printing. Mucoadhesive properties, in vitro drug release kinetics and *ex vivo* permeation rates were studied for effectiveness in drug delivery. Along with this, different techniques were used to provide insights into the surface morphology and thermal properties. The versatility of the handheld printing technology was further highlighted through its successful application on other biological macromolecules substrates that are commercially available, such as potato starch edible paper and cellulose paper, and the ability to modify printing patterns, demonstrating its full flexibility and portability.

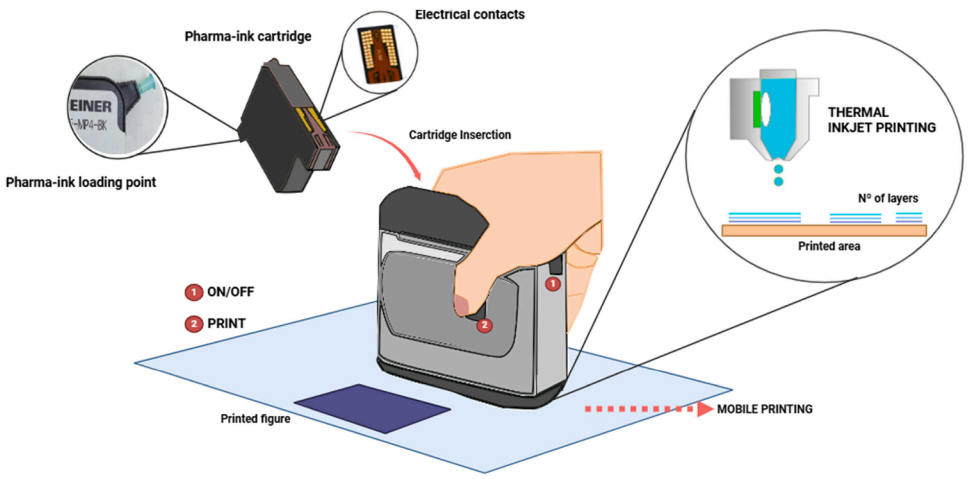

Fig. 1. Illustration of the decentralised printing process, starting with the insertion of the cartridge containing pharma-ink and depicting the handheld deposition of multiple layers of pharma-ink onto preproduced hydroxypropyl cellulose (HPC) buccal films. The diagram highlights the portable printing approach to create personalized dosage forms varying the printed area and number of layers deposited (circle on the right). The circles on the left highlight the modification made to the cartridge to include a needle for filling the cartridge with ink, while the other circle shows the cartridge electrical contacts of the handheld printer.

2. Materials and methods

2.1. Materials

(-)- Nicotine was purchased from Merck (Darmstadt, Germany); 1,2-propylene glycol (PG) was acquired from Scharlau (Barcelona, Spain); ethanol was procured from VWR International (Radnor, USA); hydroxypropyl cellulose (HPC; type M, molecular weight (MW) 700,000 g/mol) was provided from NISSO Chemical Europe GmbH (Düsseldorf, Germany); and Eudragit NE 30D was purchased from Evonik Operations GmbH (Essen, Germany). MilliQ® water was obtained using the system Milli-Q® Integral coupled with an E-POD® Dispenser 0.22 μm PES High Flux Capsule Filter from Merck (Darmstadt, Germany). Simulated saliva (pH= 6.75± 0.05) was prepared by dissolving 2.38 g Na_2HPO_4 (Scharlab S.L; Barcelona, Spain), 0.19 g KH_2PO_4 (ITW Reagents; Darmstadt, Germany) and 8.00 g NaCl (Scharlab S.L.; Barcelona, Spain) in 1000 mL of distilled water (Marques et al. 2011). Phosphate buffered saline (PBS) buffer was prepared using sodium dihydrogen phosphate anhydrous AGR (NaH_2PO_4; Labkem, Barcelona, Spain). Methanol (HPLC grade) was purchased from Merck (Darmstadt, Germany), while formic acid (99–100 %) was acquired from VWR International (Radnor, USA) Potato starch edible paper (0.3 mm thickness) was purchased from Decoración Dulce (Madrid, Spain). Cellulose paper was from The Navigator Company (Setúbal, Portugal). Bright blue colourant was purchased from Guinama (Valencia, Spain).

2.2. Pharma-inks formulation

Five pharma-inks composed of mixtures of nicotine and water were prepared, starting with 10:90 %v/v (nicotine:water) (N10:W90) and increasing by 10 % nicotine percentage until reaching 50:50 %v/v (nicotine:water) (N50:W50) (Table 1). Each ink formulation was loaded into the cartridge, and printability results were collected. This methodology allowed for the evaluation of various nicotine-water ratios for their suitability for printing.

2.3. Pharma-ink characterisation

2.3.1. Dynamic viscosity

Dynamic viscosity was measured using a Rheolyst AR 1000-N Rheometer (TA Instruments, New Castle, DE, USA) equipped with a cone-plate geometry. Measurements were conducted with a cone (ø 60 mm, angle 2.1°) on the Peltier plate set to 20 °C. Approximately 2 mL of the ink was transferred to the plate (gap of 59 μm) and subjected to a shear rate ramp from 0.05 to 1000 s^{-1} over a duration of 5 min. The viscosity value of the ink was recorded at the upper limit of the shear rate ramp (1000 s^{-1}).

Table 1
Developed pharma-inks, properties and printability results based on *Z* value.

Pharma-ink	Nicotine (%v/v)	Water (%v/v)	Density (g/mL ±SD)	Surface tension (mN/*m* ±SD)	Viscosity (mPa·s)	*Z value*
N10: W90	10	90	1.000 ± 0.003	46.48 ± 0.14	1.93	18.69
N20: W80	20	80	1.008 ± 0.002	43.61 ± 0.07	2.78	12.62
N30: W70	30	70	1.016 ± 0.002	42.73 ± 0.48	4.05	8.61
N40: W60	40	60	1.024 ± 0.007	41.85 ± 0.47	6.75	5.13
N50: W50	50	50	1.033 ± 0.004	39.40 ± 0.13	12.18	2.77

2.3.2. Surface tension

Surface tension was determined in duplicate ($n = 2$) using the platinum ring method with a Lauda Tensiometer TD1 (Lauda Scientific GmbH, Lauda-Königshofen, Germany) at room temperature.

2.3.3. Density

The density was measured ($n = 3$) using an ABT 220–4NM analytical balance (KERN & SOHN GmbH, Stuttgart, Germany). 1 mL of the ink was withdrawn using a PIPETMAN L Fixed F1000L pipette (Gilson Inc., Middleton, WI, USA) and accurately weighed at 25 °C.

2.3.4. Z value

A printability prediction was made by calculating the Z value using Eq. (1), which takes into account three physical parameters of the ink: (1) ink density (ρ, in g/mL), (2) surface tension (σ, in mN/m), and (3) viscosity (η, in mPa·s); as well as the diameter of the printer's nozzle (d, in μm) (Carou-Senra et al., 2023).

$$Z = \frac{\sqrt{\rho d \sigma}}{\eta} \quad (1)$$

2.4. Substrate preparation

Buccal films consisting of HPC and Eudragit NE30D were prepared using solvent casting, where PG was used as a plasticiser. For the preparation of the buccal films, 0.61 g of HPC was slowly added to 29.5 mL of ethanol premixed with 0.245 mL of PG under constant magnetic stirring at 200 rpm. Next, 1.73 mL of Eudragit NE 30D was incorporated into the mixture, and the stirring speed was increased to 300 rpm. The solution was stirred for 3 h to ensure a uniform blend. The mixture was then transferred into vials and sonicated for 1 h to eliminate bubbles. Finally, the blend was cast onto a Petri dish with a diameter of 13 cm^2 and dried overnight at 40 °C.

2.5. Inkjet printing (IJP)

A modified thermal inkjet cartridge (Reiner P5-MP4-BK ink, Geißler Kennzeichnungstechnik e.K. Markingshop, Norderstedt, Germany) with a nozzle diameter of 28 μm incorporated in a handheld inkjet printer (Selpic S1+, Selpic Inc., CA, USA) was used for all the printing experiments considering its easy-to-use and comfortable design. (Fig. 2). The top of the cartridge was cut with a saw, emptied, and cleaned with ethanol and distilled water. A needle was installed into the cartridge, and the pharma-inks were loaded through the needle using a syringe (Fig. 2**A**).

The printing information was transferred to the printer via Wi-Fi using the Selpic handy printer app (Selpic Inc., CA, USA), which was very intuitive and allowed users to create or upload different designs. For this study, three rectangles measuring 2.7 cm in height and 1.5, 2.5, or 3.5 cm in length (printed areas of 4.05, 6.75, and 9.45 cm^2, respectively) were created with Paint (Microsoft Inc.) and then loaded into the app (Fig. 2**C**). The printing process was performed with both single passes (1 layer) and multiple passes (up to 3 layers) of each rectangle on the films developed. The IJP was conducted under ambient conditions (21 °C) in a fume cupboard. The drug-printed films were cut following the printed dimensions and stored in Petri dishes of 9 cm^2 for further analysis.

To showcase the versatility of this portable hardware for printing on various type of substrates and design shapes, additional tests were performed on three substrates: the developed HPC buccal films, potato starch edible paper and cellulose paper. For the designs, more creative patterns such as a soccer ball, heart, and star were selected, along with QR codes and data matrices, highlighting their potential to enhance drug traceability. These shapes were printed using the N50:W50 pharma-ink, adding blue colourant to make the designs more visible.

2.6. Characterisation of the printed buccal films

2.6.1. Mechanical properties

The thickness of the films, with up to three layers, was measured from different batches using an electronic digital calliper (Max-Cal, Fowler & NSK, Fowler, UK). The results were recorded in five replicates ($n = 5$), and the mean results ± standard deviation (SD) were calculated.

2.6.1.1. Tensile strength and elongation at break. A TA.XT Plus Texture Analyser (Stable Micro Systems, Surrey, UK), equipped with a 5 kg load cell, was employed to determine the tensile strength of the drug-free and drug-printed films. Rectangular samples measuring 2.7 × 2.5 cm were secured between two clamps set 10 mm apart (**Fig. S1**). During the measurement, the strips were pulled by the top clamp at a rate of 2 mm/s. The tensile work performed during this process and the tensile elongation of the film at the moment of tearing were recorded. The tests were conducted in triplicate ($n = 3$) and results are presented as mean ± SD.

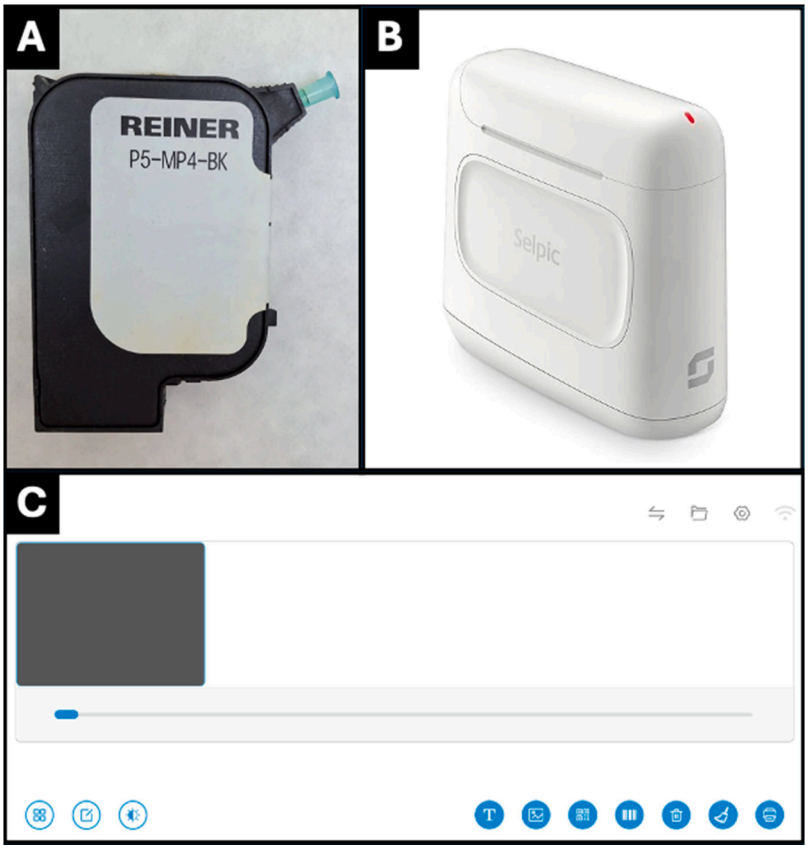

Fig. 2. Images of (A) Modified printer cartridge, P5-MP4-BK, (Ernst REINER® GmbH & Co.KG, Furtwangen, Germany), (B) Selpic S1+ handheld inkjet printer, and (C) the *Selpic handy printer* app (Selpic Inc.2.2.6, CA, USA) interface with 9.45 cm^2 rectangle load.

The elongation at break (%), tensile strength, and Young's modulus were determined using Eq. (2)-(4).

$$Elongation\ at\ break\ (\%) = \frac{Distance\ travelled}{Initial\ film\ length} \times 100 \quad (2)$$

$$Tensile\ strength = \frac{Peak\ force\ at\ break}{Film\ thickness^2} \quad (3)$$

$$Young's\ Modulus = \frac{Compressive\ stress}{Axial\ strain} \quad (4)$$

2.6.1.2. Puncture test. A TA.XT Plus Texture Analyser (Stable Micro Systems, Surrey, UK) equipped with probe P/5S (a cylindrical probe with a diameter of 5 mm) was utilised for the puncture test. The test was conducted with a 10 mm gap and a probe motion of 1 mm/s (**Figure S2**). The analyser measured the force required to puncture the 2.7 × 2.5 cm samples (puncture strength) and the deformation of the film at the moment of puncture (puncture deformation). Measurements were performed in duplicate ($n = 2$) in the drug-free and drug-printed films.

2.6.1.3. Statistical analysis. Statistical analysis was performed to compare the effect of the number of layers on the mechanical properties of the films using GraphPad (GraphPad Prism 2019, GraphPad Software, Inc, CA, USA). Given the small sample size, we assumed a non-normal distribution of the data. Therefore, a non-parametric Kruskal-Wallis test was used to compare the different test values across different film layer groups (BL, 1 Layer, 2 Layers, and 3 Layers). This test was selected as it does not assume normality and is appropriate for small sample sizes. A significance level of $p < 0.05$ was used to determine statistical differences between the groups.

2.6.2. Surface pH

Surface pH assessment of the films was conducted using drug-free and drug-printed films (2.7 × 2.5 cm) with up to 3 layers. Each film was placed in a Petri dish and 1 mL of distilled water was added to moisten the surface. Excess water was carefully removed, and then the pH on the surface of the films was evaluated using pH indicator paper (Merck KGaA, Darmstadt, Germany) placed on each specimen. Measurements were performed in duplicate ($n = 2$), and results were expressed as mean ± SD.

2.6.3. Swelling capacity

Pieces (2.7 × 2.5 cm) of drug-printed films containing up to three layers of nicotine were weighed (W_0) and individually placed in Petri dishes. Then, 5 mL of simulated saliva (composed of 2.38 g Na_2HPO_4, 0.19 g KH_2PO_4, and 8.00 g NaCl in 1 L of distilled water; pH= 6.75 ± 0.05) was added to each Petri dish. For each time point, the medium was carefully removed to weigh the film piece and replaced with fresh simulated saliva. The swelling index was calculated by measuring the change in weight at 2-min intervals until consistent values (± 0.02 g) were recorded. The tests were carried out in duplicate ($n = 2$), and the results were expressed as mean ± SD. To evaluate the effect of the number of printed layers on swelling capacity, statistical analysis was conducted using GraphPad (GraphPad Prism 2019, GraphPad Software, Inc, CA, USA). First, the Shapiro-Wilk test was used to assess the normality of the data ($p = 0.05$), and Kruskal-Wallis test was performed as a non-parametric alternative to compare the swelling capacity among the different groups.

2.6.4. X-ray powder diffraction (XRPD)

Patterns of the raw materials, drug-free and drug-printed films were recorded using a D8-Advance instrument (Bruker, Germany) equipped with a sealed X-ray tube (Cu Kα X-ray source λ = 1.5406 Å) and a LYNXEYE-type detector (Bruker, Massachusetts, USA). The intensity and voltage applied were 40 mA and 40 kV. The angular range of data acquisition was 3–50° 2θ, with a step size of 0.02° at a counting time of 2 s per step.

2.6.5. ATR-FTIR

A Spectrum 100 FTIR spectrometer (PerkinElmer, Waltham, MA) was utilised for the collection of the attenuated total reflectance-Fourier transform-infrared (ATR-FTIR) spectra. Pharma-inks, pure liquid drug solutions and excipients were measured as references for the analysis of the films. Each sample was scanned over a range of 4000–399 cm^{-1} at a resolution of 1 cm^{-1} for 6 scans.

2.6.6. Scanning electron microscopy (SEM)

The surface morphology of drug-free and drug-printed films with up to three layers was analysed using a Zeiss EVO LS15 scanning electron microscope (Zeiss, Oberkochen, Germany). Film samples were cut into small strips and mounted on aluminium specimen mounts (Electron Microscopy Science, Hatfield, PA, USA) using 12 mm Ø double-sided adhesive carbon tape. To enhance clarity of pore images, the films were gold-coated using a Q150T Plus turbomolecular pumped coater (Quorum Technologies, East Sussex, UK). Analysis was conducted at an accelerating voltage of 3.0 kV.

2.6.7. Raman spectroscopy

Drug-printed films were analysed by Raman microscopy using a WiTec Alpha 300R (Oxford Instruments, Abingdon,UK) system coupled to an CCD DU401-BVF detector at –60 °C. Raman microscopy mapping was done on the top surface to investigate the presence of nicotine throughout the depth of the film. Mapping was performed at 50x magnification using the objective Zeiss EC Epiplan-Neofluar Dic 50x/0.8. The scan depth was 90 μm, taking 100 lines per image and 150 points per line, obtaining a total of 15,000 points with an integration time of 3 s. The excitation wavelength was 531.188 nm and the laser power was 11.87 mW. The peak height at 1046 cm^{-1} was followed to determine the presence of nicotine inside the film.

2.6.8. Differential scanning calorimetry (DSC)

A Q100 differential scanning calorimeter with a refrigerated cooling accessory was used for DSC measurements (TA Instruments, New Castle, DE, USA). The films were cut into small strips and placed into aluminium pans (1 to 15 mg sample, accurately weighed using a TGA55 Discovery series precision balance; TA Instruments, New Castle, DE, USA). All measurements were conducted under nitrogen flow (50 mL/min), at a heating rate of 10 °C/min, in non-hermetic aluminium pans. The thermal analysis consisted of a heating cycle from 0 to 100 °C, followed by a cooling phase from 100 °C back to 0 °C, and then another heating phase up to 300 °C, also at 10 °C/min. Data acquisition was managed using TA Advantage software (Version 2.8), and subsequent analysis was performed utilising TA Instruments Universal Analysis 2000 (Version 4.5.0.5; TA Instruments, New Castle, DE, USA).

2.7. Drug content analysis

Drug-printed films measuring 4.05, 6.75, and 9.45 cm^2 with up to 3 layers printed were placed in vials containing 50 mL of distilled water and subjected to magnetic stirring at 250 rpm for 24 h to ensure complete dissolution. Aliquots of the medium were subsequently filtered through 0.22 μm hydrophilic filters (Millipore Ltd., Dublin, Ireland). Nicotine quantification was performed using High-Performance Liquid Chromatography (HPLC) on an Agilent system (Santa Clara, CA, USA) equipped with a Symmetry C18 5 μm 4.6 × 250 mm column (Waters, Milford, MA, USA). The analytical method for nicotine analysis was adapted from a previously published study (Meng, Lu, Gu & Xiao, 2010). The mobile phase consisted of 30:70 methanol and 0.05 % (v/v) formic acid solution, flowing at a rate of 0.6 mL/min. The column temperature was maintained at 30 °C, with an injection volume of 30 μL. Nicotine quantification was detected at a wavelength of 260 nm, and the

retention time was 8 min. All measurements were conducted in triplicate ($n = 3$), and results were expressed as mean ± SD.

2.8. In vitro drug release

Printed films measuring 4.05, 6.75, and 9.45 cm^2 with up to 3 printed layers were placed into plastic clear vials with pre-warmed (37 °C) 50 mL of simulated saliva (pH= 6.75 ± 0.05). The vials were placed in a shaker maintained at a temperature of 37 ± 0.5 °C and at shaking speed of 100 rpm. At predetermined time intervals, aliquots of the release medium (2 mL) were withdrawn and replaced with fresh medium to ensure sink conditions were maintained. The study was extended up to 24 h to ensure complete dissolution. Nicotine release was analysed using the HPLC method described in Section 2.7. For the statistical analysis of the dissolution profiles across the different layers in each area, the data distribution was assessed using the Shapiro-Wilk test and the Kruskal-Wallis test was performed to compare the dissolution profiles with significance set at $P < 0.05$ using GraphPad (GraphPad Prism 2019, GraphPad Software, Inc, CA, USA). Release profiles were analysed to determine the kinetic model that best fit the data. The Zero-order, First-order, Hixson-Crowell, Higuchi, and Korsmeyer–Peppas models were evaluated (Bruschi 2015; Siepmann & Peppas, 2011). Additionally, pure nicotine was used as a control to compare the release profiles, serving as a reference for evaluating the dissolution performance of the printed formulations.

2.9. Ex vivo permeation studies

Ex vivo buccal permeation studies of nicotine released from printed films were conducted using Franz diffusion cells with a diffusional surface area of 0.9 cm^2. Porcine buccal mucosa, sourced from a local slaughterhouse (Compostela de Carnes SL., Santiago de Compostela, Spain), was transported in PBS at pH 7.4 to the laboratory and served as the permeation barrier. Upon arrival, the non-keratinised epithelium was carefully separated from the muscle and connective tissue using a scalpel blade. Subsequently, the mucosa was trimmed to a thickness of 700 μm using surgical scissors (**Figure S3A**). The membranes were mounted on Franz diffusion cells with the epithelial side facing the donor compartment, and the receiver compartment was filled with 7 mL of PBS at pH 7.4. The diffusion cells were then placed in a temperature-controlled water bath set at 37 °C with agitation at 250 rpm for 30 min to achieve equilibrium. Next, printed films containing 1 and 3 layers of pharma-ink were attached to the tissue with the printed side facing the receiver chamber, and 500 μL of simulated saliva at pH 6.8 was added to the donor side (**Figure S3B**).

At predetermined intervals, samples of 500 μL were withdrawn from the receiver compartment and replaced with fresh PBS medium pre-warmed to 37 °C. These samples were then filtered and analysed using the HPLC method described in Section 2.7. Upon completion of the 24-h study period, a final sample was collected, and the Franz diffusion cell system was disassembled. Any remaining film residues were carefully removed and subjected to analysis to determine nicotine content by dissolving in 2 mL of distilled water. Additionally, the membrane underwent post-processing by stirring in 50 mL of methanol at 60 °C for 10 min to extract the drug, which was quantified using the HPLC method.

Permeation flux (J) was determined using Eq. (5) (Gimeno et al., 2014), as follows

$$J = \frac{dQ}{dt} \times \frac{1}{A} \tag{5}$$

J = steady state flux (mg/h/cm^2); dQ/dt = amount of drug permeated (mg/h); A = effective diffusion area (cm^2).

The permeability coefficient in cm/h was deduced by dividing the flux by the initial drug amount.

Drug permeation profiles from films with different numbers of printed layers were statistically compared using GraphPad (GraphPad Prism 2019, GraphPad Software, Inc, CA, USA). Shapiro-Wilk test was used to assess the normality of the data, Levene's test was then performed to check for homogeneity of variances. Welch's *t*-test (a variation of the independent *t*-test that does not assume equal variances) was used to determine if there were statistically significant differences between the permeation profiles of 1-layer film and 3 layer-film.

2.10. Ex vivo mucoadhesion time

The mucoadhesion of the films was evaluated using an orbital shaker (VWR Advanced Mini Shaker; VWR, PA, USA), following a protocol adapted from the literature (Yehia, El-Gazayerly & Basalious, 2009). Freshly cut porcine buccal mucosa was affixed to the side of a beaker using cyanoacrylate glue. Each film was divided into portions of 2 cm^2, and one side of each film was wetted with 50 μL of simulated saliva fluid before being applied to the porcine buccal tissue. Subsequently, the beaker was filled with 50 mL of simulated saliva at 37 °C and stirred at an approximate rate of 100 rpm to simulate buccal and saliva movement. The time taken for complete erosion or detachment of the films from the porcine membrane was recorded as the *ex vivo* mucoadhesion time.

3. Results and discussion

This study introduces a novel approach for rapid and precise preparation of personalised drug-loaded films using a handheld inkjet printer that deposits precise drug dosages on preformed polysaccharide-based films. All pharma-inks developed in this study were printable (Fig. 3). The handheld device allowed printed the inks with different shapes and sizes, including QR codes and data matrices in different substrates: a cellulose paper, a commercial orodispersible (potato starch edible paper) film, and the HPC buccal film developed specifically for this study (**Video 1 in SI file**). One of the key advantages of these portable inkjet printers is their versatility in adapting to various surfaces, thereby offering flexibility in choosing the appropriate substrate (Fig. 3**B and C**). Nonetheless, the versatility of IJP allows for intricate pattern designs, including more artistic results (Fig. 3**B**) or functional elements like QR codes or data matrices (Fig. 3**C**). Indeed, QR codes/data matrices hold promise in enhancing treatment safety and medication traceability within the pharmaceutical field (Rodríguez-Pombo et al., 2024).

Pharma-inks containing various concentrations of nicotine were formulated using distilled water as a solvent, taking advantage of the drug's complete miscibility at temperatures below 60.8 °C (Novotny & Zhao, 1999; Kheawfu et al., 2021; Krupež et al., 2018). This approach ensures formulation compatibility and aligns with the increasing demand for environmentally friendly and easily manageable drug delivery systems. The colour observed in the images (due to food colour additive) is only used to highlight the printed figures.

The pharma-inks showed variations in their rheological properties and the Z values (Table 1).The Z value, a dimensionless number widely used in IJP to predict printability based on ink rheology and nozzle diameter (28 μm), typically falls within the range of $1 < Z < 10$ (Derby, 2015). With the increase of nicotine percentage, the viscosity of the pharma-ink was higher and so did the Z value. In fact, notably, two pharma-inks evaluated in this study exceeded these conventional limits but remained printable, highlighting the complexities inherent in IJP dynamics and underscoring the need for more robust predictive tools, such as those leveraging artificial intelligence (Carou-Senra et al., 2023).

Since all developed pharma-inks were found to be printable, the formulation with the highest proportion of nicotine, N50:W50, was selected for further experiments. It is noteworthy that inks with higher nicotine content could be prepared and loaded into the printer. However, a pharma-ink with 50:50 %v/v nicotine:water ratio was suitable for the targeted doses.

In this study a film specifically designed for buccal administration

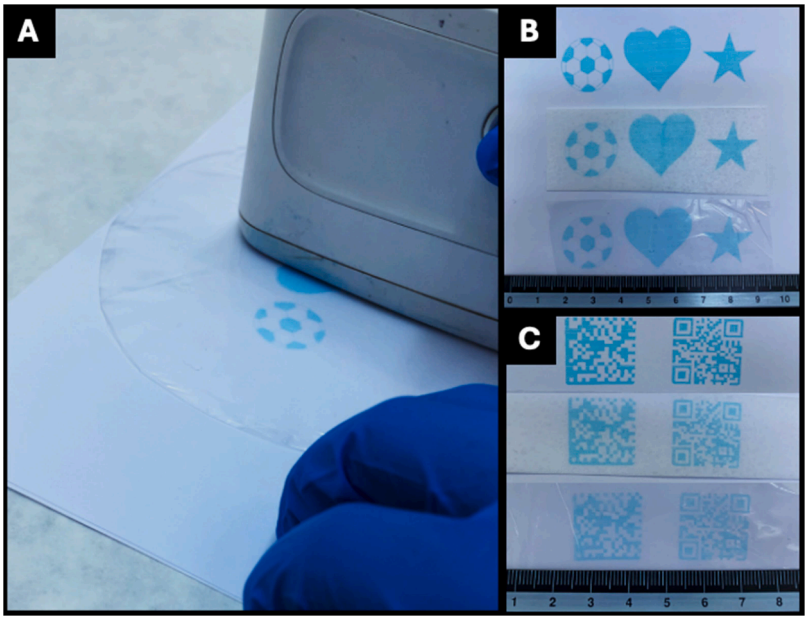

Fig. 3. Printing process of predefined figures using pharma-ink (N50:W50 + 10.6 mg blue colourant to highlight the printed figures): (A) Image during printing heart shape into the developed HPC buccal film. Results of the printing figures onto different substrates (from top to bottom): cellulose paper, potato starch edible paper, and the HPC buccal film developed in this study: (B) ball, heart and star; and (C) data matrices and QR codes.

was produced and utilised as a substrate for depositing pharma-ink using the handheld printer. Buccal films were prepared as printing substrates using the solvent casting technique (**Figure S4**). HPC and Eudragit NE 30D were chosen as main components for the films. HPC is a cellulose derivative recognised for its superior mucoadhesive properties compared to alternative synthetic film-forming agents like polyvinyl pyrrolidine or polyvinyl alcohol (Dubolazov, Nurkeeva, Mun & Khutoryanskiy, 2006; Ansari, Sadarani & Majumdar, 2018), while Eudragit NE 30D (poly(ethyl acrylate-co-methyl methacrylate) 2:1) was used to prolong retention time by reducing the solubilisation rate of the film matrix. Eudragit NE 30D is commonly used as a functional coating to endow drug dosage forms with sustained/extended release (Uboldi et al., 2023) but there are very few reports on its use as a component of films with natural macromolecules (Yehia, El-Gazayerly & Basalious, 2009). Eudragit NE 30D has 30 % content in solids. Preliminary screening of suitable compositions to prepare the films revealed that 0.61 g of HPC and 1.73 mL of Eudragit NE 30D (i.e., approx. 0.51 g polymer) provide completely transparent and swelling-controlled films, although somehow brittle. This problem was overcome with the addition of 0.245 mL of PG. This composition is in line with a previous report on films from pectin and Eudragit NE 30D for transdermal delivery, in which the best mass ratios were found to be 1:0.5 and 1:1 (Yehia, El-Gazayerly & Basalious, 2009). However, in that previous study, glycerin was used as plasticizer at 30 % w/w based on polymers contents, while we observed that PG at 21 % w/w was sufficient.

Also, unlike other methodologies where the drug is incorporated directly into the polymer mixture before casting, in the present work, the model drug was printed onto pre-produced films. This approach circumvents conventional limitations such as batch-to-batch variability due to drug effects on polymer miscibility or curing process, ensuring

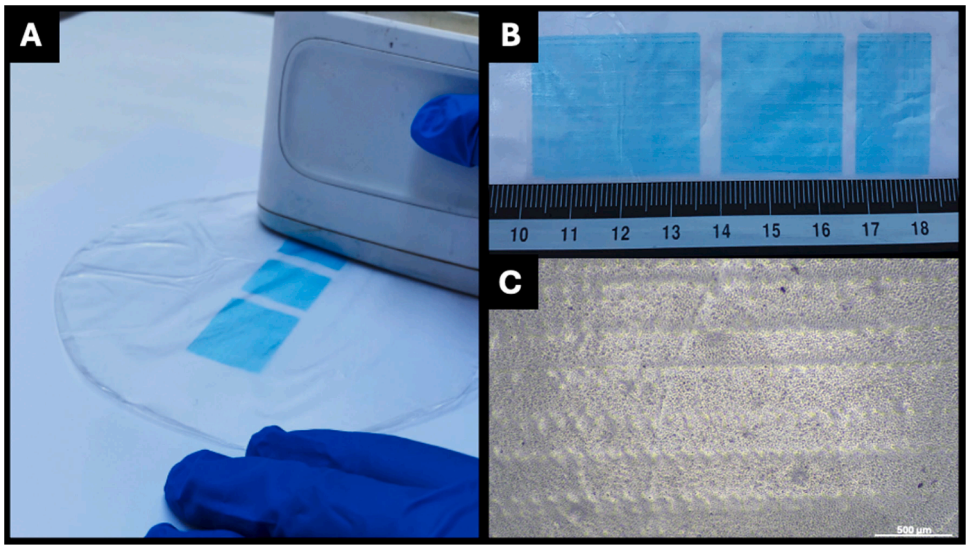

Fig. 4. Images of the films printed with the developed pharma-ink (N50:W50) onto the developed HPC buccal films: (A) Image during printing of the predefined 3 rectangles with pharma-ink (N50:W50 + 10.6 mg blue colourant). (B) Printed buccal films with areas 4.05, 6.75 and 9.45 cm^2 with pharma-ink (N50:W50 + 10.6 mg blue colourant). Scale shown in cm. (C) Optical microscope image of 1 layer film with pharma-ink (N50:W50). Scale: 500 µm.

higher homogeneity of the printed films (Carou-Senra et al., 2024), and also makes HPC/Eudragit films ready-to-use substrates where any drug could be printed.

Following substrate preparation, rectangles of predefined dimensions were printed using the developed pharma-ink (N50:W50) (Fig. 4**A and B**). The printed area was subsequently trimmed carefully, and the films were stored in Petri dishes for further analysis. For this study, a simpler geometric shape was chosen to maximise printed area, with patient comfort being a priority.

During the study, up to three layers of pharma-ink were deposited onto the films. Films with a single layer display rows composed of small dots (Fig. 4**C**). Drug doses between 0.6 and 4.3 mg were achieved varying area and the number of printed layers (Table 2). Commercially available buccal formulations of nicotine (gums, lozenges and sprays) provided crafted doses of 1, 1.5, 2 and 4 mg; thus, doses achieved in this study were therapeutically relevant. The amount of drug deposited increased proportionally with both the printer area and the number of layers. Thus, higher printed doses can be obtained by increasing these parameters.

The consistency of the inkjet printing process for drug deposition on the HPC films was quantified in terms of the drug deposited per unit area (cm^2) under standardised conditions, such as the smallest area of 4.05 cm^2 with one layer (0.15 mg/cm^2). From this baseline condition, the expected drug deposition for different areas and layers was estimated by multiplying the area by the number of layers printed, and the recovery was calculated. By comparing the estimated doses with the experimental doses achieved, the printing reproducibility was assessed. The close alignment between calculated and achieved doses indicated high consistency of the IJP process, with estimated recoveries ranging between 95 % and 102 % (Table 2). This suggests a rapid scaling-up process for producing personalised drug-loaded films with accurate, on-demand doses. The linear relationship between drug dose, printed area, and printed layers allows for straightforward calculation of the required area and number of layers to achieve a desired dose with high accuracy. This flexibility enables doses to be tailored to individual patient requirements simply by adjusting these two parameters.

Regarding the ATR-FTIR spectra (Fig. 5), HPC exhibits stretching vibrations bands related to C—O groups located at 1075–1175 cm^{-1}, bands corresponding to aliphatic groups located at 2800–2950 cm^{-1}, and bands corresponding to -OH appeared around 3500 cm^{-1} (Eguchi, Kawabata & Goto, 2017; Davies, 2023). These bands were also observed in the drug-free and drug-printed films containing up to 3 layers. Eudragit exhibited characteristic bands of the C═O ester vibration at 1730 cm^{-1}, which were also present in the drug-free films and drug-printed films with up to 3 layers (Lin, Augsburger, Muhammad & Pope, 2001). In the nicotine FTIR spectrum, the C—H stretching was observed between 2969 and 2780 cm^{-1}. The aromatic C═N double bond stretching appeared as a peak around 1585 cm^{-1}, while the aromatic C═C double bond stretching was observed around 1653 cm^{-1}. Additionally, peaks at 712 cm^{-1} and 884 cm^{-1}, corresponding to the out-of-plane bending of the C—H bond of the monosubstituted pyridinic cycle, were evident in the nicotine spectrum (Al-Dahhan et al., 2021). These peaks were slightly attenuated in the pharma-ink spectrum due to the formulation containing 50 % water. Comparing the peaks in the spectra of pure nicotine and pharma-ink with the developed films, it appears that the peaks at 712 cm^{-1} and 884 cm^{-1} were observable in the printed films but not in the drug-free films or the pure HPC spectrum. Similarly, the peak around 1653 cm^{1} was also observed only in the printed films, not in the drug-free films, indicating the presence of nicotine in the developed buccal films. XRPD transmission diffractograms of drug-free and 3 layers-printed buccal films (**Figure S5**) revealed an amorphous structure, consistent with the non-crystalline nature of HPC.

Table 2
Number of layers of the deposited ink, amount of drug deposited onto each area, the estimated drug dose and the calculated estimated recovery (%). Mean values ± standard deviations ($n = 3$).

Printed Area (cm^2)	Number of Layers	Dose Mean (mg±SD)	Estimated dose (mg)	Estimated Recovery (%±SD)
4.05	1	0.61 ± 0.01	0.61	100.00 ± 1.25
	2	1.16 ± 0.01	1.22	95.06 ± 0.20
	3	1.82 ± 0.00	1.83	99.61 ± 0.11
6.75	1	1.04 ± 0.01	1.02	102.70 ± 1.05
	2	2.02 ± 0.05	2.03	100.27 ± 2.46
	3	3.01 ± 0.07	3.05	98.73 ± 2.45
9.45	1	1.42 ± 0.04	1.42	99.74 ± 3.07
	2	2.85 ± 0.00	2.84	100.06 ± 0.15
	3	4.29 ± 0.07	4.27	100.66 ± 1.56

SEM analyses were conducted to investigate the surface morphology of the developed buccal films, both without drug and with up to 3 layers of pharma-ink (Fig. 6). Drug-free films exhibited a predominantly smooth surface interspersed with pores (Fig. 6**A**). However, with the introduction of successive drug layers, the surface morphology underwent a notable transformation. The pores visible in the drug-free film gradually filled as the number of drug layers increased. Additionally, surface roughness increased with each additional layer of pharma-ink deposited. Particularly, films containing 3 printed layers showed significantly pronounced roughness (Fig. 6**D**).

Raman microscopy was used to examine nicotine distribution in the film to determine whether the drug remained on the surface or penetrated the film. The peak height at 1046 cm^{1} could be tentatively assigned to the trigonal ring deformation of pyridine and used to determine nicotine distribution through the film (Chien et al., 2020; Tian et al., 2021). Results showed that despite the greater presence of nicotine close to the surface, the drug migrated towards the interior. Drug migration increased when increasing the number of layers printed (Fig. 7).

Mechanical properties of the buccal films were also evaluated. Thickness measurements across different batches, including both drug-free films and films with up to 3 layers of pharma-ink, consistently ranged from 0.02 mm to 0.03 mm (**Table S1**). The number of layers did not significantly increase the thickness of the films, as each layer consists of only picoL-sized droplets. Given the small volume of each droplet and their incorporation into the polymer matrix, the overall thickness did not increase substantially. Moreover, the thinness of these films provided excellent flexibility, allowing them to conform to various surfaces, such as the buccal mucosa. This flexibility facilitated the deposition of pharma-ink using the Selpic printer, and the film surface did not impede the printer's movement during the printing process.

Films printed with pharma-ink demonstrated higher elasticity and lower brittleness compared to drug-free films, as evidenced by the results of the elongation at break (Fig. 8**A**) and tensile strength (Fig. 8**B**) tests, respectively. Additionally, printed films exhibited greater stiffness than drug-free films, as indicated by Young's moduli (Fig. 8**C**). The mechanical properties were dependent on the number of printed layers, with lower elongation observed for 2 and 3 layers (statistically significant; $p = 0.0014$), resulting in slightly higher tensile strength and Young's modulus ($p < 0.05$). These differences indicate that the number of printed layers has a significant effect on these parameters.

Puncture tests were conducted to determine the force required to puncture the buccal films and the deformation at break. The results indicated that puncture strength slightly decreased when the number of printed layers increased, reflecting the transition of HPC to a softer state probably due to the plasticising effect of nicotine (Fig. 8**D**). However, the decrease in strength was not substantial (particularly noticeable for 1 and 2 layers), where properties remained comparable to those of the drug-free film. In terms of deformation, it slightly increased with the number of printed layers (Fig. 8**E**), but no statistically significant differences were found.

Considering that nicotine films come into direct contact with the oral cavity and their pH can potentially induce irritation to the oral mucosa,

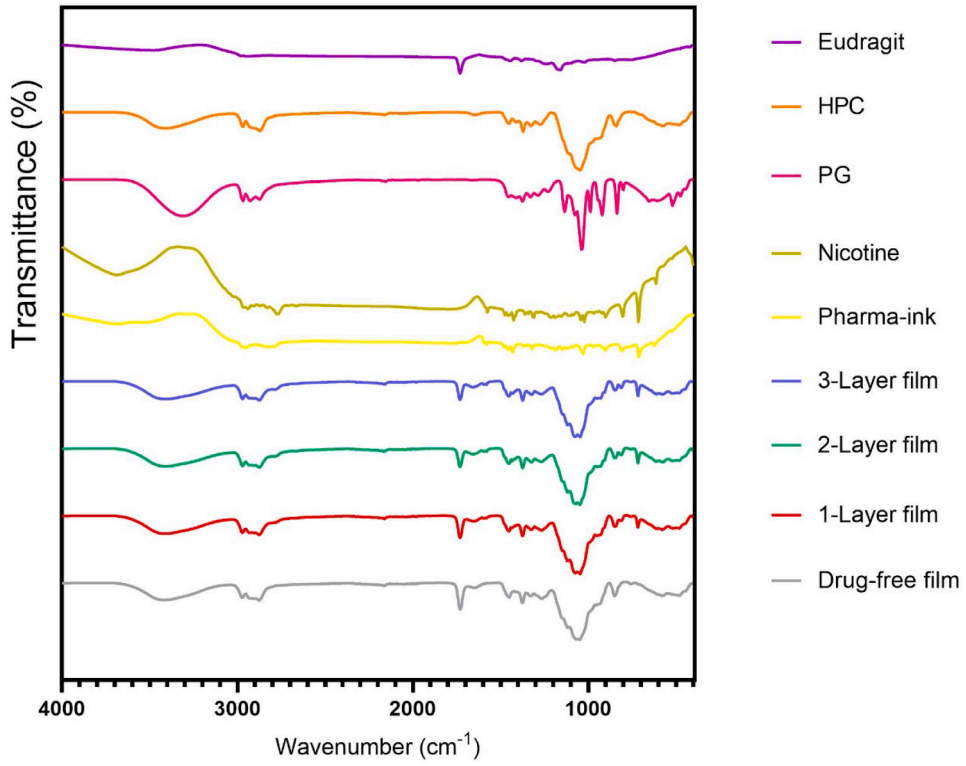

Fig. 5. ATR-FTIR spectra of pure nicotine, pure excipients, pharma-ink, drug-free film and different films printed up to 3 layers.

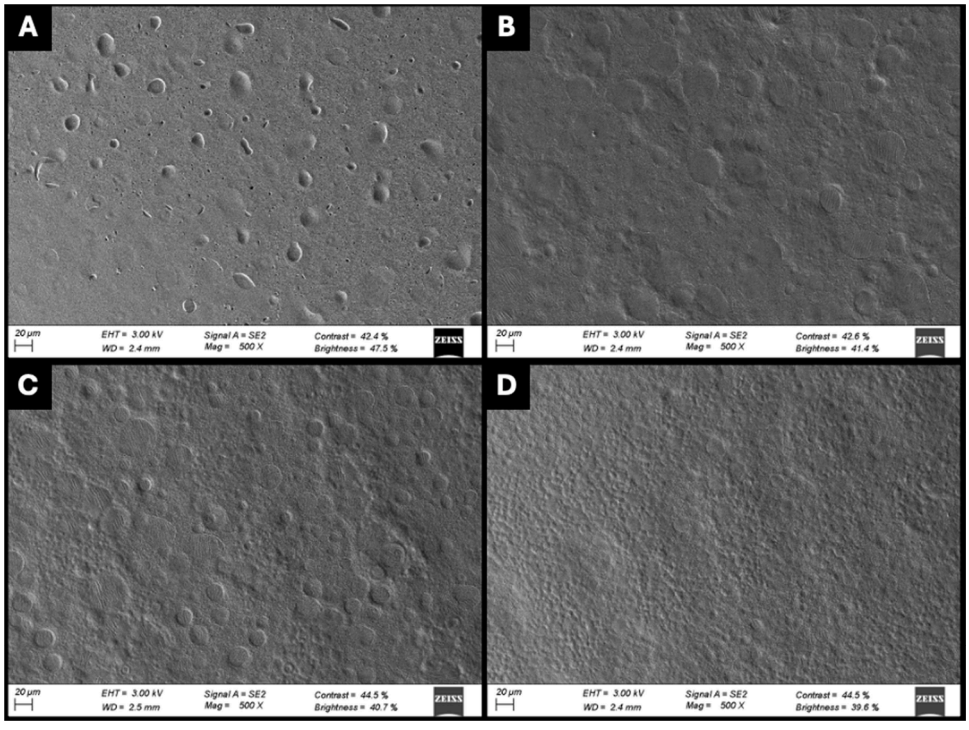

Fig. 6. SEM images of the surface morphology of HPC films with different printed layers: (A) drug-free film, (B) 1-layer printed film, (C) 2-layer printed film, and (D) 3-layer printed film. Scale: 20 μm.

the surface pH of both drug-free films and films printed with 3 layers of nicotine was determined. The pH of the surface of drug-free films was measured to be approximately 6. When the number of printed layers increased, the pH increased slightly, from 7 for the 1-layer and 2-layer printed films to pH 8 for the 3-layer printed films. This alkaline microenvironment may facilitate the penetration of nicotine through the buccal mucosa and into the bloodstream. The swelling index of both the drug-free and 3-layer-printed buccal films revealed rapid uptake of simulated saliva within the initial few minutes of testing (4 min), after which sorption stabilised (Fig. 9). The Shapiro-Wilk test confirmed that

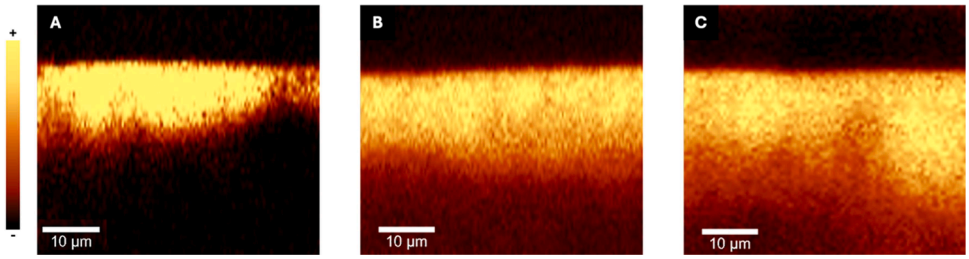

Fig. 7. Raman mapping of nicotine distribution across the film: (A) 1-layer film, (B) 2-layer film and, (C) 3-layer film. Images were taken from the upper surface, extending 90 µm depth. The image was processed to adjust for the film's actual thickness. The colour bar indicates density of nicotine concentration, with '+' representing areas of higher drug concentration and '-' indicating areas of lower drug concentration. Scale bar: 10 µm.

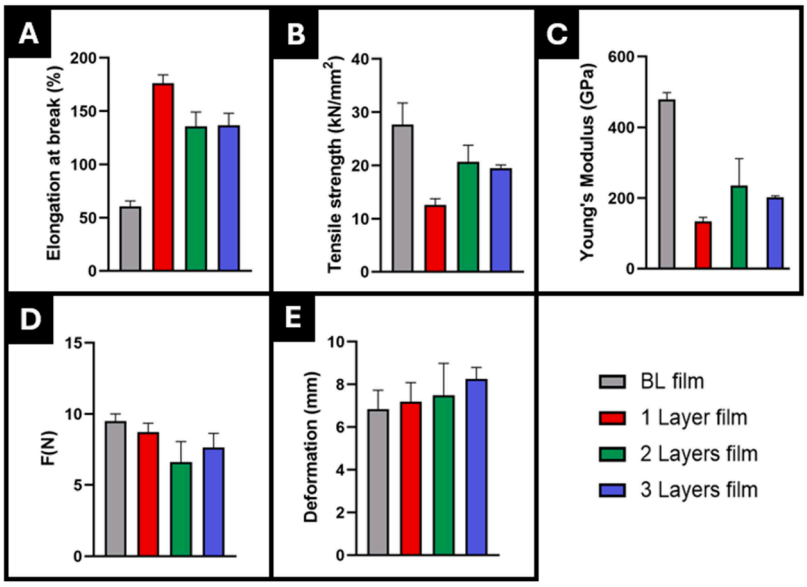

Fig. 8. Mechanical properties of buccal films showing the effect of pharma-ink layers on: (A) elongation at break (%), (B) tensile strength (kN/mm^2), (C) Young's modulus (GPa), (D) puncture strength (N); and (E) puncture deformation (mm) of the buccal films showing the effect of different pharma-ink layers.

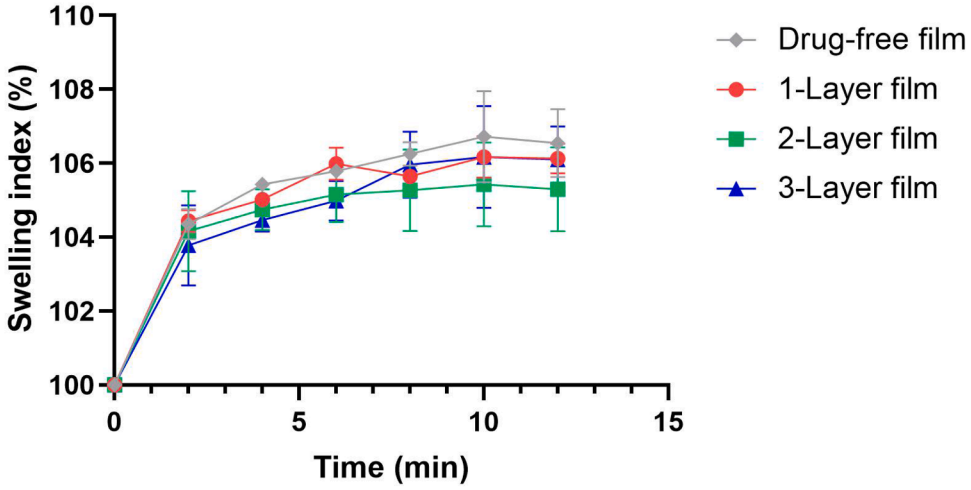

Fig. 9. Swelling profiles of the nicotine-free, 1-, 2- and 3-layer buccal films in simulated saliva at pH= 6.75 ± 0.05.

the data did not follow a normal distribution, ($p < 0.05$). Given this, the Kruskal-Wallis test was applied, yielding a statistic of 2.64 and a p-value of 0.45. Since $p > 0.05$, no statistically significant differences were observed between groups. These results indicate that the number of printed layers did not significantly affect the swelling capacity.

The in vitro release tests of nicotine from mucoadhesive films were conducted on films printed with the three different areas: 4.05 cm^2 (Fig. 10**A**), 6.75 cm^2 (Fig. 10**B**), and 9.45 cm^2 (Fig. 10**C**). Each figure illustrates how the number of printed layers (up to 3 layers) influenced the drug release profile for each area. It was observed that in each case,

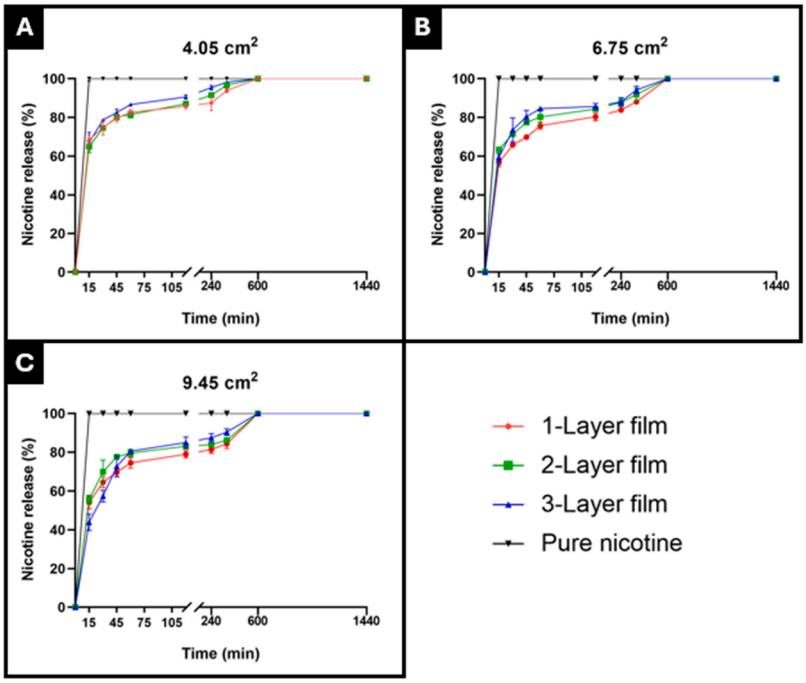

Fig. 10. In vitro release profiles of nicotine from the (A) 4.05 cm^2, (B) 6.75 cm^2, and (C) 9.45 cm^2 buccal films in simulated saliva pH= 6.75 ± 0.05. Pure (free) nicotine was used as a control.

there was an initial burst release within the first 15 min, with >40 % of nicotine released from the buccal films. This was followed by a decrease in the release rate observed over the subsequent hours. Control tests carried out with nicotine doses equivalent to those printed in the three layers of each area showed 100 % dissolution within the first 15 min (Fig. 10). Therefore, incorporation of nicotine in the films provided more sustained release.

The number of printed layers did not significantly change the drug release process, although an increase in the printed area corresponded with a slight decrease in drug release. This effect could be likely due to the mucoadhesive properties of the buccal film, which may lead to adhesion to the vessel walls or to itself, thereby reducing the effective exposed area for drug release. Also, it could be due to the higher penetration of nicotine in the bulk of the film. However, these effects did not significantly impact overall drug release, indicating that increasing the number of layers did not lead to substantial changes in the drug release behaviour across the tested areas (no statistically significant differences; $p > 0.5$). Additionally, release profiles were analysed to determine the kinetic model that best fit the data. The Zero-order, First-order, Hixson-Crowell, Higuchi, and Korsmeyer–Peppas models were evaluated, and their parameters are presented in **Table S2**. Upon analysis, the release profiles showed a closer fit to the Korsmeyer-Peppas model, followed by the First-order model, which exhibited the highest R^2 values. This finding aligns with expectations, as the Korsmeyer-Peppas model is specifically suited for describing drug release from polymer matrices. The values of 'n' in the Korsmeyer-Peppas model were predominantly <0.5, suggesting that drug release was governed by a diffusion-controlled mechanism which aligns with Raman results exhibiting that nicotine was not just on the surface, but also embedded in the polymeric matrix of the film (Fig. 6).

Understanding drug release behaviour is crucial in pharmaceutical development, as it directly impacts the absorption and therapeutic efficacy of the agent (Ramteke, Dighe, Kharat & Patil, 2014). However, standardised test methods and specifications for oromucosal film preparation and dissolution testing remain lacking (Speer, Preis & Breitkreutz, 2019). Consequently, various approaches have been adopted across studies, leading to significant variability. Factors such as the choice of apparatus - including paddle, basket, paddle-over-disk, Franz diffusion cell, or vials - and variations in test volumes further contribute to this heterogeneity (Pongjanyakul & Suksri, 2009; Okeke & Boateng, 2016). In this study, we deliberately avoided large volumes as they do not accurately reflect oral conditions, opting instead for simulated saliva as a medium to closely mimic the physiological environment.

The results of the *ex vivo* permeation studies using porcine buccal mucosa comparing 1 layer-printed and 3 layers-printed films are illustrated in Fig. 11. According to the theoretical conditions set for drug content studies, where 0.15 mg of nicotine was intended to be printed per cm^2 and layer, an expected content of 0.135 mg per layer was anticipated for the diffusion area of the Franz cells (0.9 cm^2).

In the initial hour of the experiment, approximately 12 % of the dose crossed the mucosa, reaching 50 % after 5 h. By the end of the 24-h study period, a total of 0.123 mg of nicotine had permeated through the mucosa. Analysis of both the buccal mucosa and the remaining film in the donor compartment confirmed concentrations below our quantification limit (<0.033 μg/mL), suggesting that 91.1 % of the nicotine permeated through the membrane. For the 3 layers-printed films, where the theoretical nicotine amount printed was 0.405 mg, about 8 % of the nicotine crossed the membrane within the first hour. Similar to the 1-layer films, around 50 % of the nicotine had permeated the porcine membrane after 5 h. At the conclusion of the 24-h study, a total of 0.403 mg of nicotine had crossed the mucosa. Analysis of the mucosa revealed the presence of 0.01 mg of nicotine, while analysis of the film remains did not yield detectable results due to the minute remnants of the film and nicotine, so a theoretical 98.3 % of the nicotine permeated through the membrane.

The permeability profiles showed a slower permeation over time compared to the release tests, which can be attributed to the fundamental differences between the two processes. While dissolution tests measure the release of the drug from the formulation into the medium, ex vivo permeation is governed by the diffusion of the released drug through the mucosal membrane, which acts as a natural barrier, limiting the rate of drug transport. This difference results in a more gradual and sustained permeation profile rather than the rapid release observed in dissolution studies. These findings are consistent with previous studies that have developed films containing the same drug, where similar

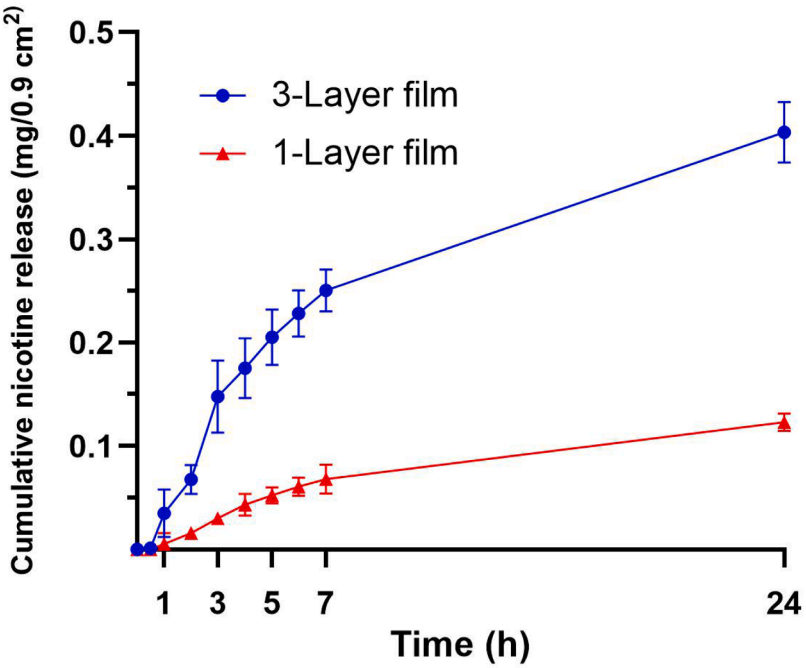

Fig. 11. *Ex vivo* permeation of nicotine from the 3-layer and 1-layer buccal mucoadhesive films.

permeability behaviours have been reported (Pongjanyakul & Suksri, 2009; Boateng & Okeke, 2019).

Flux of free nicotine through porcine mucosa has been previously evaluated covering a very wide range of conditions, obtaining values in the 0.160 to 0.260 mg/h/cm^2 (Cornaz Gudet, Ganem-Quintanar & Buri, 1997). In our case, nicotine flux for films with a single layer was 0.012 mg/h/cm^2, while for films containing 3 layers of pharma-ink this flux increased to 0.056 mg/h/cm^2. These values are in the range of those reported for other nicotine buccal formulations tested in porcine tissue (Boateng & Okeke, 2019). The fact of that the permeability increased for films with more layers of pharma-ink (statistically significant differences; $p = 0.024$) is related to the greater amount of drug loaded, supplying higher initial drug concentration in the donor chamber. Moreover, as demonstrated in other tests (Fig. 6), the printed layers might alter the surface of films facilitating easier diffusion. In the same way, the permeability coefficients where 0.05 cm/h and 0.08 cm/h, for 1-layer films and 3-layer films respectively.

However, it is important to note the numerous challenges in replicating oral cavity conditions. *Ex vivo* permeation studies using animal buccal mucosa can be influenced by factors such as the choice of animal species, mucosal integrity, viability, and thickness. Additionally, despite being widely used and informative, Franz diffusion cells have limitations, particularly in mimicking saliva flow rates. Salivary flow rates vary widely among individuals, with normal unstimulated flow rates typically above 0.1 mL/min. In this study, due to the small volume in the receiver compartment and the need to maintain sink conditions, 500 μL of saliva was added to the donor compartment to moisten the films. Despite efforts to isolate the compartment with parafilm, this volume was mostly absorbed over time, leading to drying, reduced mucosal viability, and potentially affecting drug permeation rate (Adrover, Pedacchia, Petralito & Spera, 2015).

Overall, the films exhibited close adhesion to the mucosal surface, with no detachment observed during the initial hours of testing. Upon exposure to the medium, which took advantage of the films' swelling properties mentioned earlier, the films transitioned to a soft state and adhered firmly to the membrane. Throughout the first 4 h of testing, no remnants of the film were observed in the medium. By the 5-h mark, slight peeling was noted at the film ends, but adherence remained intact. Visible erosion began around the 7-h mark, with small remnants of film visible in the middle but a thin layer still adhered to the mucosa. It is important to note that the volume used in these experiments exceeds typical oral cavity conditions, accelerating the disintegration and swelling processes of the films. Nevertheless, the films maintained close adhesion to the mucosa without detachment during the initial phase of the test. Buccal films with varying residence times have been reported in the literature, with some formulations showing adhesion for a few hours, others reaching up to 4 h (Patel, Prajapati & Patel, 2007), and some achieving prolonged adhesion times between 6 and 8 h (Yehia, El-Gazayerly & Basalious, 2009; Jain, Jain, Gupta & Kharya, 2008). Our formulation demonstrated a residence time of 7 h, which places it within the range of extended adhesion times observed in other studies. This result is highly positive, as it suggests that our film maintains good adhesion while ensuring a prolonged release period, which is desirable for buccal drug delivery systems.

For the first time, a handheld inkjet printer has been successfully used in the pharmaceutical field for the decentralised production of buccal films containing patient-centric nicotine doses. This portable hardware enabled precise deposition of personalised drug amounts onto preproduced substrates, offering a flexible and decentralised approach to personalised medicine production on-demand. Nicotine buccal films have gained attention in recent years as an appealing alternative to other dosage forms. So far, those nicotine-loaded films were developed by the solvent casting technique by adding the drug directly in the polymer mixture (Suksaeree et al., 2021; W.a.P. Khunawattanakul, 2024). Consequently, these conventional methods often exhibit high variability in drug content (Carou-Senra et al., 2024). Preparation of drug-printed buccal films using IJP has been previously explored in other studies with promising results that overcame these limitations (G. Eleftheriadis et al., 2020; G.K. Eleftheriadis et al., 2020). However, this time the printer used enabled hassle-fee, portable and on-demand printing right at your fingertips, just being able to personalise precisely the drug dose by changing only two parameters: area and layers of pharma-ink printed. Regarding improvements in the nicotine replacement therapy, films produced showed a great buccal absorption, that could avoid the first-hepatic pass, something that gums or lozenges on the market cannot accomplish. Furthermore, the precision of the IJP technique itself and the flexibility of the novel hardware can allow individualized doses to be printed in seconds. In this scenario, on-demand production can support

gradual cessation plans by adjusting just the two mentioned parameters. This approach enables precise dose customisation for each patient within seconds, allowing for quick and easy modifications over time. As a result, therapeutic outcomes can be enhanced, and the treatment can be better tailored to each patient's needs. Additionally, a controlled release was achieved which could satisfied cravings initially and sustained the effect for several hours. It has been determined that drug release is not influenced by the number of layers in the films. However, it may be affected by the type of polymeric matrix used. For instance, buccal formulations with higher amounts of sodium alginate have exhibited a rapid release with 92 ± 8 % of nicotine released within the first 30 mins wafers (Okeke & Boateng, 2016), while other buccal formulations containing other types of Eudragit and pectin exhibited a more sustained release of nicotine (Suksaeree et al., 2021).

Although these dosage forms were produced in a laboratory, the capabilities of this portable inkjet printer allow for their production in various settings, including hospitals, community pharmacies, and even at home, bringing personalised medicine closer to patients. In hospital settings, a portable printer could enable medical staff to quickly and efficiently produce necessary medications; in community pharmacies could leverage this technology to offer bespoke medication in a precise and automatic manner; for home use, these devices empower patients to manage some of their treatments more effectively, improving treatment adherence. It also presents an appealing option for medicine production in underdeveloped or remote areas (Seoane-Viaño, Ong, Basit & Goyanes, 2022), where other types of equipment are less accessible. In fact, handheld inkjet printers offer a cost-effective solution for small-scale pharmaceutical needs by significantly reducing infrastructure and operational costs, while also minimising energy consumption making them an environmentally friendly option (Carou-Senra et al., 2024).

It is important to recognise that, as a proof-of-concept, further research is needed to develop a handheld inkjet printer specifically designed for pharmaceutical applications, ensuring compliance with Good Manufacturing Practices (GMP) to facilitate its adaptation for clinical studies. Moreover, integrating a healthcare software which could easily automate the scale of figures to obtain the required dose and the number of layers needed. The integration of technologies such as QR codes or data matrices for medication traceability could enhance patient safety by ensuring accurate dosage tracking and verification (Rodríguez-Pombo et al., 2024; Öblom et al., 2020; Edinger et al., 2018). Moreover, exploring this approach with other drugs could further establish its potential and lead to the development of decentralised medications, while the combination of this portable hardware with sustainable substrates can be a good alternative for producing other pharmaceutical applications, as its versatility has been demonstrated during the study.

4. Conclusion

In this study, a handheld inkjet printer was introduced for the mobile production of personalised medicines—specifically, buccal films containing flexible doses of nicotine for nicotine replacement therapy were printed on-demand on HPC films by varying number of layers and area printed. This innovative application of IJP technology enables the precise and reproducible fabrication of pharmaceutical dosage forms tailored to individual therapeutic needs and treatment progress, aiming to enhance treatment effectiveness. Moreover, the portability of the handheld inkjet printer allows for the convenient production of these drug-loaded buccal films in diverse settings, thereby promoting ease of access and patient adherence. Its versatility has also been showcased across various substrates, enabling a broad range of applications.

The developed buccal HPC films exhibited a controlled release profile characterised by an initial burst release followed by sustained release, offering potential advantages in maintaining therapeutic drug levels over extended periods. Comprehensive evaluations of HPC films containing up to three printed layers encompassed assessments of mechanical properties, swelling behaviour, and mucoadhesive characteristics, complemented by detailed surface analyses using advanced optical techniques. These insights highlight IJP as a promising technology for the precise development of personalised medicines, heralding a new era in pharmaceutical research and development.

The integration of handheld IJP technology facilitates the straightforward, adaptable, and patient-specific production of films containing various drug and doses, tailoring therapies to individual needs. The versatility and mobility provided by handheld printers and ready-to-use eco-friendly substrates will streamline medication administration and enhance treatment outcomes, potentially revolutionising personalised medicine delivery. This study not only highlights the capabilities of IJP in pharmaceutical development but also sets a precedent for future innovations aimed at advancing therapeutic efficacy and patient care through personalised drug delivery systems.

CRediT authorship contribution statement

Paola Carou-Senra: Writing – review & editing, Writing – original draft, Visualization, Software, Methodology, Investigation, Formal analysis, Data curation, Conceptualization. **Atheer Awad:** Writing – review & editing, Writing – original draft, Visualization, Software, Methodology, Investigation, Formal analysis, Conceptualization. **Abdul W. Basit:** Writing – review & editing, Visualization, Supervision, Resources, Methodology, Conceptualization. **Carmen Alvarez-Lorenzo:** Writing – review & editing, Writing – original draft, Validation, Supervision, Resources, Project administration, Methodology, Investigation, Funding acquisition, Formal analysis, Conceptualization. **Alvaro Goyanes:** Writing – review & editing, Writing – original draft, Validation, Supervision, Resources, Project administration, Methodology, Investigation, Funding acquisition, Formal analysis, Conceptualization.

Declaration of competing interest

The authors declare the following financial interests/personal relationships which may be considered as potential competing interests: Carmen Alvarez-Lorenzo reports equipment, drugs, or supplies was provided by Spain Ministerio de Ciencia e Innovación. Paola Carou-Senra reports financial support was provided by Government of Galicia Department of Education Science Universities and Professional Training. Alvaro Goyanes reports a relationship with FABRX Ltd. that includes: consulting or advisory. Abdul W. Basit reports a relationship with FABRX Ltd. that includes: consulting or advisory. If there are other authors, they declare that they have no known competing financial interests or personal relationships that could have appeared to influence the work reported in this paper.

Acknowledgements

PCS acknowledges the Predoctoral Fellowship [Programa de axudas á etapa predoutoral, grant number [ED481A 2023] from Xunta de Galicia (Consellería de Cultura, Educación, Formación Profesional e Universidades) co-funded by the European Union under the framework of the FSE+ Galicia 2021–2027 Program.

Funding: The work was supported by Spain Ministerio de Ciencia e Innovación MCIN/AEI/10.13039/501100011033 [PID2023-149544OB-C22, PID2023-150422OB-I00], FEDER and Xunta de Galicia [ED431C 2024/09].

Supplementary materials

Supplementary material associated with this article can be found, in the online version, at doi:10.1016/j.carpta.2025.100724.

Data availability

Data will be made available on request.

References

A.C. Society, Nicotine Replacement Therapy to Help You Quit Tobacco. https://www.cancer.org/cancer/risk-prevention/tobacco/guide-quitting-smoking/nicotine-replacement-therapy.html, 2021 (16th of July).

Adrover, A., Pedacchia, A., Petralito, S., & Spera, R. (2015). In vitro dissolution testing of oral thin films: A comparison between USP 1, USP 2 apparatuses and a new millifluidic flow-through device. *Chemical Engineering Research & Design: Transactions of the Institution of Chemical Engineers, 95*, 173–178. https://doi.org/10.1016/j.cherd.2014.10.020

Al-Dahhan, W. H., Kadhom, M., Yousif, E., Mohammed, S. A., & Alkaim, A. (2021). Extraction and determination of nicotine in tobacco from selected local cigarettes brands in Iraq. *Letters in Applied NanoBioScience, 11*, 3278–3290.

Allen, A. M., Yuan, N. P., Wertheim, B. C., Krupski, L., Bell, M. L., & Nair, U. (2019). Gender differences in utilization of services and tobacco cessation outcomes at a state quitline. *Translational Behavioral Medicine, 9*, 663–668. https://doi.org/10.1093/tbm/iby083

Alomari, M., Vuddanda, P. R., Trenfield, S. J., Dodoo, C. C., Velaga, S., Basit, A. W., et al. (2018). Printing T3 and T4 oral drug combinations as a novel strategy for hypothyroidism. *International Journal of Pharmaceutics, 549*, 363–369. https://doi.org/10.1016/j.ijpharm.2018.07.062

Ansari, M., Sadarani, B., & Majumdar, A. (2018). Optimization and evaluation of mucoadhesive buccal films loaded with resveratrol. *Journal of Drug Delivery Science and Technology, 44*, 278–288. https://doi.org/10.1016/j.jddst.2017.12.007

Boateng, J., & Okeke, O. (2019). Evaluation of clay-functionalized wafers and films for nicotine replacement therapy via buccal mucosa. *Pharmaceutics, 11*, 104. https://doi.org/10.3390/pharmaceutics11030104

5 - Mathematical models of drug release. In Bruschi, M. L. (Ed.), *Strategies to modify the drug release from pharmaceutical systems*, (pp. 63–86). (2015) (pp. 63–86). Woodhead Publishing.

Buanz, A. B. M., Saunders, M. H., Basit, A. W., & Gaisford, S. (2011). Preparation of personalized-dose salbutamol sulphate oral films with thermal ink-jet printing. *Pharmaceutical Research, 28*, 2386–2392. https://doi.org/10.1007/s11095-011-0450-5

Carou-Senra, P., Ong, J. J., Castro, B. M., Seoane-Viano, I., Rodríguez-Pombo, L., Cabalar, P., et al. (2023). Predicting pharmaceutical inkjet printing outcomes using machine learning. *International Journal of Pharmaceutics: X, 5*, Article 100181. https://doi.org/10.1016/j.ijpx.2023.100181

Carou-Senra, P., Rodríguez-Pombo, L., Awad, A., Basit, A. W., Alvarez-Lorenzo, C., & Goyanes, A. (2024). Inkjet printing of pharmaceuticals. *Advanced materials (Deerfield Beach, Fla), 36*, Article 2309164. https://doi.org/10.1002/adma.202309164

Carpenter, M. J., Jardin, B. F., Burris, J. L., Mathew, A. R., Schnoll, R. A., Rigotti, N. A., et al. (2013). Clinical strategies to enhance the efficacy of nicotine replacement therapy for smoking cessation: A review of the literature. *Drugs, 73*, 407–426. https://doi.org/10.1007/s40265-013-0038-y

Chien, J.-Y., Gu, Y.-C., Tsai, H.-M., Liu, C.-H., Yen, C.-Y., Wang, Y.-L., et al. (2020). Rapid identification of nicotine in electronic cigarette liquids based on surface-enhanced Raman scattering. *Journal of Food and Drug Analysis, 28*, 302. https://doi.org/10.38212/2224-6614.1064

Cornaz Gudet, A. L., Ganem-Quintanar, A. F., & Buri, P. (1997). Simple method of in vitro diffusion of nicotine across porcine palatine mucosa. *European Journal of Pharmaceutics and Biopharmaceutics: Official Journal of Arbeitsgemeinschaft fur Pharmazeutische Verfahrenstechnik eV, 43*, 259–264. https://doi.org/10.1016/S0939-6411(97)00049-0

Davies, M. A. (2023). Rotational isomerism of the side chains of hydroxypropyl cellulose in aqueous solution observed using attenuated total reflectance infrared spectroscopy. *Spectroscopy Journal, 1*, 111–120. https://doi.org/10.3390/spectroscj1030010

Derby, B. (2015). Additive manufacture of ceramics components by inkjet printing. *Engineering, 1*, 113–123. https://doi.org/10.15302/J-ENG-2015014

Dubolazov, A. V., Nurkeeva, Z. S., Mun, G. A., & Khutoryanskiy, V. V. (2006). Design of mucoadhesive polymeric films based on blends of poly (acrylic acid) and (hydroxypropyl) cellulose. *Biomacromolecules, 7*, 1637–1643. https://doi.org/10.1021/bm060090l

Edinger, M., Bar-Shalom, D., Sandler, N., Rantanen, J., & Genina, N. (2018). QR encoded smart oral dosage forms by inkjet printing. *International Journal of Pharmaceutics, 536* (1), 138–145. https://doi.org/10.1016/j.ijpharm.2017.11.052

Eguchi, N., Kawabata, K., & Goto, H. (2017). Electrochemical polymerization of 4, 4-dimethyl-2, 2'-bithiophene in concentrated polymer liquid crystal solution. *Journal of Chemical Engineering and Materials Science, 5*, 64–70. https://doi.org/10.4236/msce.2017.52007

Eleftheriadis, G., Monou, P. K., Andriotis, E., Mitsouli, E., Moutafidou, N., Markopoulou, C., et al. (2020a). Development and characterization of inkjet printed edible films for buccal delivery of B-complex vitamins. *Pharmaceuticals, 13*, 203.

Eleftheriadis, G. K., Monou, P. K., Bouropoulos, N., Boetker, J., Rantanen, J., Jacobsen, J., et al. (2020b). Fabrication of mucoadhesive buccal films for local administration of ketoprofen and lidocaine hydrochloride by combining fused deposition modeling and inkjet printing. *Journal of Pharmaceutical Sciences, 109*(9), 2757–2766. https://doi.org/10.1016/j.xphs.2020.05.022

Flowers, L. (2017). Nicotine replacement therapy. *The American Journal of Psychiatry Residents' Journal*. https://doi.org/10.1176/appi.ajp-rj.2016.11060

Fox, C. B., Nemeth, C. L., Chevalier, R. W., Cantlon, J., Bogdanoff, D. B., Hsiao, J. C., et al. (2017). Picoliter-volume inkjet printing into planar microdevice reservoirs for low-waste, high-capacity drug loading. *Bioengineering & Translational Medicine, 2*, 9–16. https://doi.org/10.1002/btm2.10053

Gardes, J., Maldivi, C., Boisset, D., Aubourg, T., Vuillerme, N., & Demongeot, J. (2019). Maxwell®: An unsupervised learning approach for 5P medicine. *MEDINFO 2019: Health and wellbeing e-networks for all* (pp. 1464–1465). IOS Press.

Genina, N., Fors, D., Vakili, H., Ihalainen, P., Pohjala, L., Ehlers, H., et al. (2012). Tailoring controlled-release oral dosage forms by combining inkjet and flexographic printing techniques. *European Journal of Pharmaceutical Sciences: Official Journal of the European Federation for Pharmaceutical Sciences, 47*, 615–623. https://doi.org/10.1016/j.ejps.2012.07.020

Gimeno, A., Calpena, A. C., Sanz, R., Mallandrich, M., Peraire, C., & Clares, B. (2014). Transbuccal delivery of doxepin: Studies on permeation and histological investigation. *International Journal of Pharmaceutics, 477*, 650–654. https://doi.org/10.1016/j.ijpharm.2014.10.060

Hang, R.. What can a handheld inkjet printer do for you?. https://www.heatsign.com/what-can-a-handheld-inkjet-printer-do-for-you/.

Jain, S. K., Jain, A., Gupta, Y., & Kharya, A. (2008). Design and development of a mucoadhesive buccal film bearing progesterone. *Die Pharmazie-An International Journal of Pharmaceutical Sciences, 63*, 129–135. https://doi.org/10.1691/ph.2008.7114

Kheawfu, K., Kaewpinta, A., Chanmahasathien, W., Rachtanapun, P., & Jantrawut, P. (2021). Extraction of nicotine from tobacco leaves and development of fast dissolving nicotine extract film. *Membranes, 11*(6), 403. https://doi.org/10.3390/membranes11060403

Kosmider, M. D. L., Koszowski, B., Sobczak, A., Benowitz, N. L., & Goniewicz, M. L. (2018). Slower nicotine metabolism among postmenopausal Polish smokers. *Pharmacological Reports : PR, 70*(3), 434–438. https://doi.org/10.1016/j.pharep.2017.11.009

Krueger, L., Awad, A., Basit, A. W., Goyanes, A., Miles, J. A., & Popat, A. (2024). Clinical translation of 3D printed pharmaceuticals. *Nature Reviews Bioengineering*, 1–3. https://doi.org/10.1038/s44222-024-00217-x

Krupež, J., Kovačević, V. V., Jović, M., Roglić, G. M., Natić, M. M., Kuraica, M. M., et al. (2018). Degradation of nicotine in water solutions using a water falling film DBD plasma reactor: Direct and indirect treatment. *Journal of Physics D: Applied Physics, 51*(17), Article 174003. https://doi.org/10.1088/1361-6463/aab632

Kumria, R., Nair, A. B., Goomber, G., & Gupta, S. (2016). Buccal films of prednisolone with enhanced bioavailability. *Drug Delivery, 23*, 471–478.

Lin, A. Y., Augsburger, L. L., Muhammad, N. A., & Pope, D. (2001). Study of crystallization of endogenous surfactant in eudragit NE30D-free films and its influence on drug-release properties of controlled-release diphenhydramine HCl pellets coated with eudragit NE30D. *AAPS Pharmsci, 3*, 57–68. https://doi.org/10.1208/ps030214

Meher, J. G., Tarai, M., Yadav, N. P., Patnaik, A., Mishra, P., & Yadav, K. S. (2013). Development and characterization of cellulose–polymethacrylate mucoadhesive film for buccal delivery of carvedilol. *Carbohydrate Polymers, 96*, 172–180. https://doi.org/10.1016/j.carbpol.2013.03.076

Meng, X. J., Lu, L. L., Gu, G. F., & Xiao, M. (2010). A novel pathway for nicotine degradation by Aspergillus oryzae 112822 isolated from tobacco leaves. *Research in Microbiology, 161*, 626–633. https://doi.org/10.1016/j.resmic.2010.05.017

Montenegro-Nicolini, M., Miranda, V., & Morales, J. O. (2017). Inkjet printing of proteins: An experimental approach. *The AAPS Journal, 19*, 234–243. https://doi.org/10.1208/s12248-016-9997-8

NHS, Stop smoking treatments. https://www.nhs.uk/conditions/stop-smoking-treatments/, (accessed 23 September 2024).

Novotny, T. E., & Zhao, F. (1999). Consumption and production waste: Another externality of tobacco use. *Tobacco Control, 8*, 75–80. https://doi.org/10.1136/tc.8.1.18

Öblom, H., Cornett, C., Bøtker, J., Frokjaer, S., Hansen, H., Rades, T., et al. (2020). Data-enriched edible pharmaceuticals (DEEP) of medical cannabis by inkjet printing. *International Journal of Pharmaceutics, 589*, Article 119866. https://doi.org/10.1016/j.ijpharm.2020.119866

Okeke, O. C., & Boateng, J. S. (2016). Composite HPMC and sodium alginate based buccal formulations for nicotine replacement therapy. *International Journal of Biological Macromolecules, 91*, 31–44. https://doi.org/10.1016/j.ijbiomac.2016.05.079

Olsson Gisleskog, P. O., Perez Ruixo, J. J., Westin, Å., Hansson, A. C., & Soons, P. A. (2021). Nicotine population pharmacokinetics in healthy smokers after intravenous, oral, buccal and transdermal administration. *Clinical Pharmacokinetics, 60*, 541–561. https://doi.org/10.1007/s40262-020-00960-5

Patel, V. M., Prajapati, B. G., & Patel, M. M. (2007). Effect of hydrophilic polymers on buccoadhesive Eudragit patches of propranolol hydrochloride using factorial design. *AAPS PharmSciTech, 8*, E119–E126.

Pongjanyakul, T., & Suksri, H. (2009). Alginate-magnesium aluminum silicate films for buccal delivery of nicotine. *Colloids and Surfaces B: Biointerfaces, 74*, 103–113. https://doi.org/10.1016/j.colsurfb.2009.06.033

Ramteke, K. H., Dighe, P. A., Kharat, A. R., & Patil, S. V. (2014). Mathematical models of drug dissolution: A review. *Scholars Academic Journal of Pharmacy, 3*, 388–396.

Rodríguez-Pombo, L., Carou-Senra, P., Rodríguez-Martínez, E., Januskaite, P., Rial, C., Félix, P., et al. (2024). Customizable orodispersible films: Inkjet printing and data matrix encoding for personalized hydrocortisone dosing. *International Journal of Pharmaceutics, 655*, Article 124005. https://doi.org/10.1016/j.ijpharm.2024.124005

Sandler, N., Määttänen, A., Ihalainen, P., Kronberg, L., Meierjohann, A., Viitala, T., et al. (2011). Inkjet printing of drug substances and use of porous substrates-towards individualized dosing. *Journal of Pharmaceutical Sciences, 100*, 3386–3395. https://doi.org/10.1002/jps.22526

Schnoll, R. A., Patterson, F., & Lerman, C. (2007). Treating tobacco dependence in women. *Journal of Women's Health, 16*, 1211–1218. https://doi.org/10.1089/jwh.2006.0281

Semalty, M., Semalty, A., & Kumar, G. (2008). Formulation and characterization of mucoadhesive buccal films of glipizide. *Indian Journal of Pharmaceutical Sciences, 70*, 43.

Seoane-Viaño, I., Ong, J. J., Basit, A. W., & Goyanes, A. (2022). To infinity and beyond: Strategies for fabricating medicines in outer space. *International Journal of Pharmaceutics: X, 4*, Article 100121. https://doi.org/10.1016/j.ijpx.2022.100121

Siepmann, J., & Peppas, N. A. (2011). Higuchi equation: Derivation, applications, use and misuse. *International Journal of Pharmaceutics, 418*, 6–12. https://doi.org/10.1016/j.ijpharm.2011.03.051

Speer, I., Preis, M., & Breitkreutz, J. (2019). Dissolution testing of oral film preparations: Experimental comparison of compendial and non-compendial methods. *International Journal of Pharmaceutics, 561*, 124–134. https://doi.org/10.1016/j.ijpharm.2019.02.042

Suksaeree, J., Chaichawawut, B., Srichan, M., Tanaboonsuthi, N., Monton, C., Maneewattanapinyo, P., et al. (2021). Applying design of experiments (DoE) on the properties of buccal film for nicotine delivery. *e-Polymers, 21*, 566–574. https://doi.org/10.1515/epoly-2021-0064

Tian, Y., Tang, X., Fu, Y., Shang, S., Dong, G., Li, T., et al. (2021). Simultaneous extraction and surface enhanced Raman spectroscopy detection for the rapid and reliable identification of nicotine released from snus products. *Analytical Methods, 13*, 5608–5616. https://doi.org/10.1039/D1AY01601F

Tracy, T., Wu, L., Liu, X., Cheng, S., & Li, X. (2023). 3D printing: Innovative solutions for patients and pharmaceutical industry. *International Journal of Pharmaceutics, 631*, Article 122480. https://doi.org/10.1016/j.ijpharm.2022.122480

Uboldi, M., Gelain, A., Buratti, G., Gazzaniga, A., Melocchi, A., & Zema, L. (2023). Development of 4D printed intravesical drug delivery systems: Scale-up of film coating. *Journal of Drug Delivery Science and Technology, 87*, Article 104875. https://doi.org/10.1016/j.jddst.2023.104875

Vogler, S., Zimmermann, N., Haasis, M. A., Knoll, V., Espin, J., Mantel-Teeuwisse, A. K., et al. (2024). Innovations in pharmaceutical policies and learnings for sustainable access to affordable medicines. *Journal of Pharmaceutical Policy and Practice, 17*, Article 2335492. https://doi.org/10.1080/20523211.2024.2335492

W.a.P. Khunawattanakul, T. (2024). Chitosan− magnesium aluminum silicate nanocomposite− based films of nicotine for buccal delivery: Mixing order effect and drug retention. *Journal of Drug Delivery Science and Technology, 92*, Article 105266. https://doi.org/10.1016/j.jddst.2023.105266

WHO, Regulation and prequalification. https://www.who.int/teams/regulation-prequalification/lpa, (accessed 1 January 2025).

Yehia, S. A., El-Gazayerly, O. N., & Basalious, E. B. (2009). Fluconazole mucoadhesive buccal films: In vitro/in vivo performance. *Current Drug Delivery, 6*, 17–27. https://doi.org/10.2174/156720109787048195